Ultramicroscopy 129 (2013) 30–35

Contents lists available at SciVerse ScienceDirect

Ultramicroscopy

journal homepage: www.elsevier.com/locate/ultramic

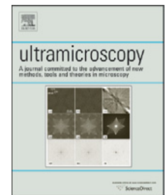

Spatial high resolution energy dispersive X-ray spectroscopy on thin lamellas

Christian Notthoff [a,*], Markus Winterer [a], Andreas Beckel [b], Martin Geller [b], Jürgen Heindl [c]

[a] Lehrstuhl Nanopartikel-Prozesstechnik and CeNIDE, Universität Duisburg-Essen, Lotharstrasse 1, D-47057 Duisburg, Germany
[b] Fakultät für Physik and CeNIDE, Universität Duisburg-Essen, Lotharstrasse 1, D-47057 Duisburg, Germany
[c] JEOL (Germany) GmbH, Oskar-v.-Miller-Str. 1a, D-85386 Eching, Germany

ARTICLE INFO

Article history:
Received 4 May 2012
Received in revised form
1 February 2013
Accepted 9 February 2013
Available online 18 February 2013

Keywords:
EDX
SEM
FIB
Monte-Carlo

ABSTRACT

For conventional samples and measurement geometries the spatial resolution of energy dispersive X-ray spectroscopy is limited by a tear drop shaped emission volume to about 1 μm. This restriction can be substantially improved using thin samples and high acceleration voltage. In this contribution the spatial resolution of energy dispersive X-ray spectroscopy in a scanning electron microscope using thin lamella samples is investigated. At an acceleration voltage of 30 kV, an edge resolution down to $\Delta d_{edge} = 40 \pm 10$ nm is observed performing linescans across an interface, using an 80 nm thin sample prepared from a GaAs/AlAs-heterostructure. Furthermore, Monte-Carlo simulations of pure elements ranging from sodium to mercury are performed for different sample thicknesses. From the simulations we can derive a simple empirical formula to predict the spatial resolution as a function of sample thickness.

© 2013 Elsevier B.V. All rights reserved.

1. Introduction

Spatially resolved imaging of elemental distributions using scanning electron microscopes (SEM) or transmission electron microscopes (TEM) plays a key role in many scientific fields like semiconductor physics or material science and also in industrial standards for the routine quality and failure analysis [1]. Modern aberration corrected TEMs are able to resolve element specific informations down to the atomic scale [2], however, the sample preparation and measurement are much more demanding and TEMs are much less available than SEMs. In SEMs, one common method to obtain spatially resolved element specific information of a bulk sample is energy dispersive X-ray analysis (EDX) detecting the characteristic X-rays generated while the focused electron beam is scanned across the sample. The continuous further development of SEM's now allows resolutions down to 1 nm in imaging mode, while in classical EDX mode the resolution is still restricted to about 1 μm. The reason behind this restriction is the elastic and/or inelastic scattering of the electrons inside the sample, which leads to a large tear-drop like excitation volume where characteristic X-rays are generated. The depth t and the lateral extension r of the excitation volume can be described by the well-known Castainge's formulas [4,5]

$$t\,(\mathrm{nm}) = 33 \cdot (E_0^{1.7} - E_c^{1.7}) \cdot \frac{A}{\rho \cdot Z}, \tag{1}$$

$$r\,(\mathrm{nm}) = \frac{0.4114 \cdot Z^{2/3}}{1 + 0.187 \cdot Z^{2/3}} \cdot t, \tag{2}$$

where E_0 is the acceleration voltage of the incident electron beam in kV, E_c is the minimum emission voltage in keV, A is the averaged atomic mass, Z is the averaged atomic number and ρ is the density of the sample. Assuming a laterally structured but homogeneous in-depth sample for simplicity, the resolution in quantitative EDX-analysis is directly proportional to the lateral extent of the X-ray emission volume, because the material composition of a feature is predicted correctly only if the entire X-ray emission volume is within this feature (see e.g. [3,4]). As can be seen from the above formulas, one possibility to improve the spatial resolution in the EDX analysis is the reduction of the acceleration voltage [4,6], which results in a smaller excitation volume. For example, Barkshire et al. [4] report a plateau resolution of 40 nm measured on a Ni/AuCu-heterostructure using 5 kV acceleration voltage. One major disadvantage of a low acceleration voltage is that the K-lines of most elements are no longer accessible and the measurements are restricted to low-energy L-/M-lines. The low-energy lines are generally less well separated from each other and are theoretically more poorly described than K-lines.

Another way described in the literature (see e.g. Ref. [7]) to increase the spatial resolution in the SEM is the use of thin lamellas instead of bulk samples e.g. prepared by a focused ion beam (FIB). This will reduce the interaction volume geometrically without a reduction of the acceleration voltage.

In this paper we present high resolution EDX-measurements on a GaAs/AlAs-heterostructure and investigate the dependence

* Corresponding author. Tel.: +49 0203 379 3144.
E-mail address: christian.notthoff@uni-due.de (C. Notthoff).

0304-3991/$ - see front matter © 2013 Elsevier B.V. All rights reserved.
http://dx.doi.org/10.1016/j.ultramic.2013.02.008

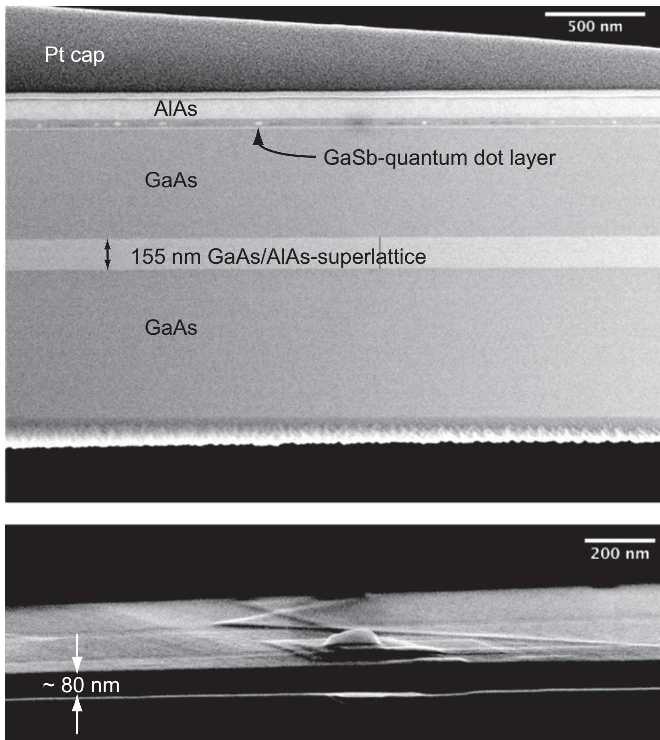

Fig. 1. STEM-image of a thin GaAs/AlGaAs FIB-lamella at an acceleration voltage of 30 kV (top) and the side view in secondary electron imaging mode (bottom).

of the physical resolution limits on the sample material and thickness using Monte-Carlo simulations.

2. Experimental

A JEOL-JSM7500F cold field emission SEM with a scanning transmission detector (STEM) in dark field mode was used for the imaging. An acceleration voltage of 30 kV and a probe current of ~6 nA was used for all experiments. A Bruker Quantax 200 system equipped with a 30 mm^2 SSD crystal is attached to the SEM for the EDX measurements. For the EDX-measurements a ~80 nm thin lamella was prepared from a molecular beam epitaxial grown GaAs/AlAs-heterostructure by a combined FIB/SEM instrument of the type FEI Helios Nanolab.

A dark field STEM image of the sample is shown in Fig. 1 (top) together with a side view of the lamella (bottom). The GaAs/AlAs-heterostructure consists of a 740 nm GaAs bottom layer, followed by a 155 nm AlAs/GaAs-superlattice with 1 nm modulation and a 550 nm GaAs layer. The top layers also include a self-assembled gallium antimony (GaSb) quantum dot layer, which are not investigated here in detail.

3. Results and discussion

Fig. 2 shows a typical EDX-spectrum averaged over the measurement points of a linescan across the GaAs surrounded GaAs/AlAs-superlattice accumulated for 5 min at an acceleration voltage of 30 kV. We observe only a very low bremsstrahlung background which vanishes already at photon energies $> 7-8$ keV, while the characteristic X-ray emission lines are well developed. At high energies, the As-K (10.5 keV), the Ga-K (9.2 keV) and a Cu-K (8 keV) emission lines can be identified. The observed copper signal is an artifact from the support of the FIB-lamella.

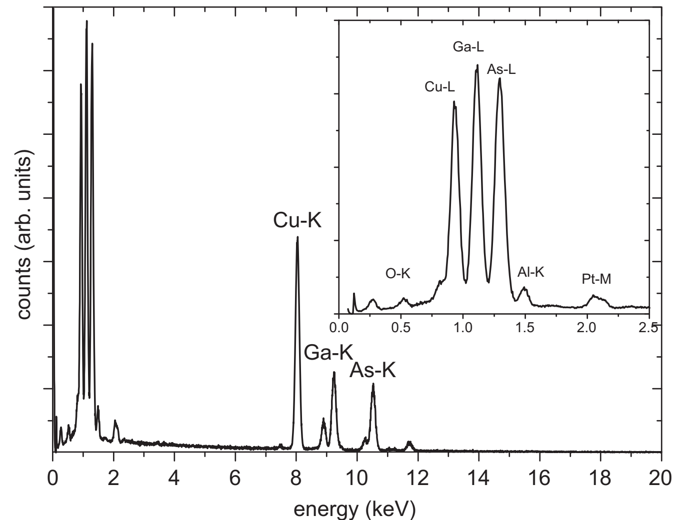

Fig. 2. EDX-spectrum of the FIB-lamella at 30 kV acceleration voltage accumulated for 5 min. The inset enlarges the energy range below 2.5 keV.

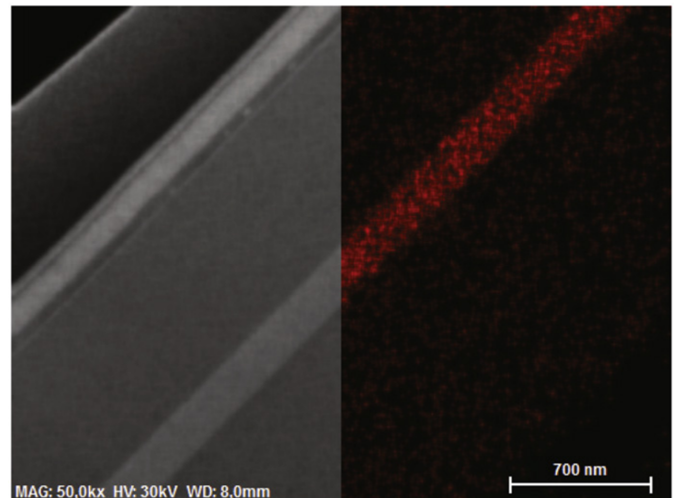

Fig. 3. STEM-image of the FIB-lamella at a magnification of 50,000, acceleration voltage of 30 kV and a working distance of 8 mm (left) and the corresponding aluminum EDX-signal accumulated for 25 min (right).

The inset enlarges the energy range below 2.5 keV where the Pt-M (2.1–2.3 keV), the Al-K (1.5 keV) and a O-K (0.5 keV) emission lines are observed. The L-lines of Ga, As and Cu are also located in this energy range. The reduced bremsstrahlung background compared to bulk samples is a direct result of the small interaction volume of the electron beam with the thin sample. Therefore, we expect a high material contrast in quantitative EDX-linescan and mapping measurements. We would like to note that for standardless quantification algorithms, used in most of the common evaluation software (like Esprit), the bremsstrahlung background is essential for a correct determination of material composition, making them unsuitable here. For a standardless quantification of material compositions new algorithms are needed taking into account the finite sample thickness. Alternatively, one can use the well-established Cliff–Lamor method [8], which is a standard based quantification method known from transmission electron microscopy.

Fig. 3 shows a STEM dark field image of the lamella on the left side and the corresponding quantitative aluminum map accumulated for 20 min on the right. In the STEM image Al rich areas

appear bright. As already expected from the EDX-spectrum (see Fig. 2) we observe a very good material contrast in the qualitative EDX-mapping of the aluminum in our lamella ($SNR \approx 5$). Besides a well-developed material contrast and the intrinsic resolution limits of the sample which we discuss later on it is extremely important to get the SEM under optimal operating conditions to achieve the highest spatial resolution in EDX-measurements. One critical parameter is the stability of the beam current over time. The emitter of a cold field emission SEM needs to be 'flashed' from time to time and shows a characteristic variation of the beam current over time. Only in a certain time slot, typically 2–3 h after a 'flash', the beam current is stable enough to allow EDX-measurements with more than 20 min averaging time. At high magnification it is nearly impossible to avoid a small image shift caused over time e.g. by thermal drifts or due to the glue used to fix the sample. Modern EDX-software provides advanced drift correction algorithms to actively compensate for such small drift motions of the sample. However, these algorithms depend on well-resolved structures in the SEM image.

As suggested by Barkshire et al. [4], one way of quantifying the spatial resolution in EDX-analysis is to perform linescans across a sharp, well-defined interface of two materials. Fig. 4 illustrates the situation schematically. The contribution of material B to the total emission is illustrated as a shaded area inside the excitation volume (bottom), together with the resulting contribution of an characteristic emission line of material B to the EDX-signal (top). For such a linescan the edge resolution Δd_{edge} is typically defined as the distance between the points where the EDX signal increases from 10% to 90% of the step height, indicated as dashed lines in Fig. 4. Therefore, we have performed EDX-linescans across the well-defined GaAs/AlAs-superlattice (shown in Fig. 3) to quantify the resolution which can be obtained in our JSM7500F microscope together with the Quantax 200 system. Fig. 5 shows a typical linescan for the aluminum and the gallium signals (blue solid lines) at a magnification of 100,000 and 30 kV acceleration voltage. The aluminum signal shows a very steep increase from the background level to the plateau value within less than 50 nm as indicated by the gray shaded area in Fig. 5. The valley in the gallium signal appears slightly broader than the aluminum

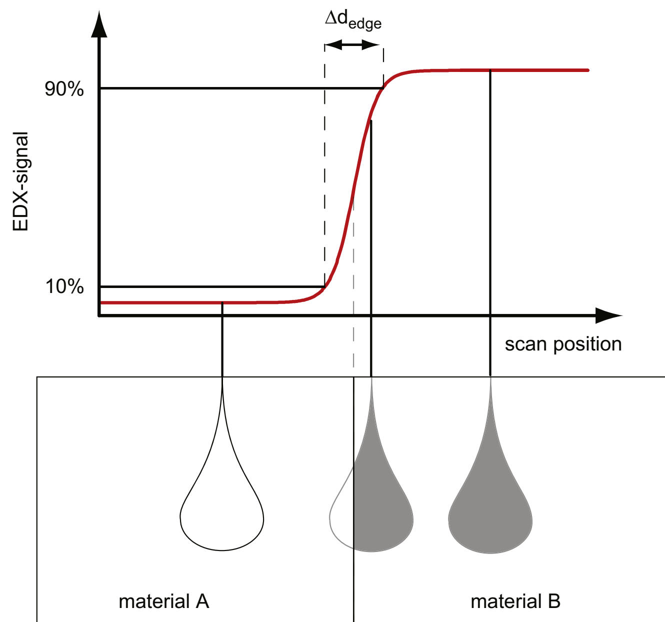

Fig. 4. Illustration of an EDX-linescan across a sharp interface of two materials A and B (bottom) and the resulting contribution of material B to the EDX-signal, together with the definition of edge resolution used herein.

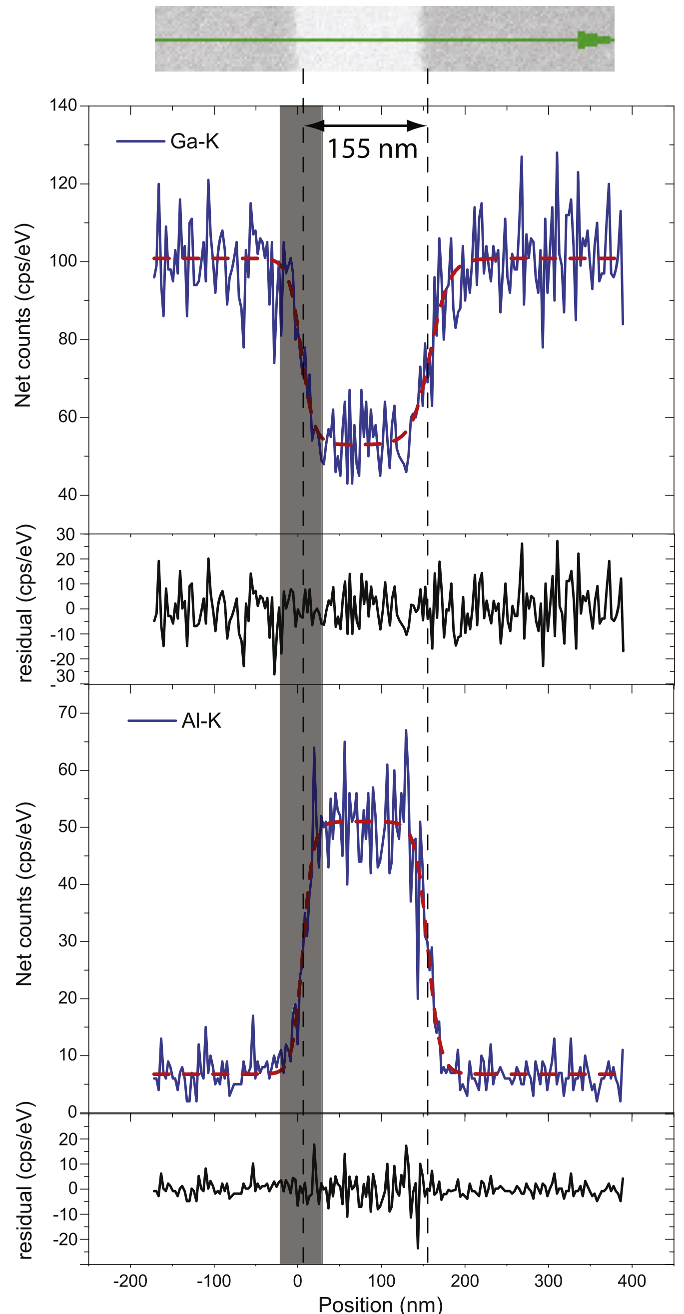

Fig. 5. EDX-linescan across the AlAs/GaAs-superlattice (blue solid lines) together with the corresponding STEM image (top) and a fit to the experimental data (red dashed lines). The arrow in the image indicates the scan direction and position. Details are given in the text. (For interpretation of the references to color in this figure caption, the reader is referred to the web version of this article.)

plateau, because the compositional contrast for gallium is 50% less than for aluminum inside the GaAs/AlAs-superlattice.

To quantify the edge resolution from the EDX-linescans we have fitted the smooth function [9]

$$I(x) = \beta + \gamma \left(\frac{1}{1+\exp\left(\frac{x-x_2}{w_2}\right)} - \frac{1}{1+\exp\left(\frac{x-x_1}{w_1}\right)} \right) \tag{3}$$

to the aluminum and the gallium signals, which directly yields the edge resolution $\Delta d_{edge} = 4.39 \cdot w_i$. Here $w_1$and w_2 are fit parameters for the steepness of the edges, β fits the base line and γ represents the step height of the plateau. In addition to the edge resolution, we obtain the plateau width $d_{EDX} = |x_2 - x_1|$ of the

aluminum rich layer, which compared with the width determined by the STEM-image also provides a measure of resolution. The results of six linescans at different positions are summarized in Table 1. All fits show a reasonable coefficient of determination (R^2) and a quite good signal-to-noise ratio (SNR), taking into account the short measurement time of 600 s and the low overall count rate. The average of the fits yields a plateau width of $d_{plateau} = 156 \pm 4$ nm for both the Al-K and Ga-K signals. Therefore, the width of Al-rich area determined from the STEM image ($d_{SEM} = 155 \pm 1$ nm) is reproduced by the EDX linescan with a resolution of $\Delta d_{plateau} = \pm 4$ nm. For the edge resolution we obtain $\Delta d_{edge} = 40 \pm 10$ nm from the EDX linescans as indicated with the gray shaded area in Fig. 5. It is interesting to note that the edge resolution obtained for the left and right edges of the GaAs/AlAs-superlattice shows a significant difference of up to 17 nm while the plateau width does not show a significant variation, which is an indication of an image shift during a linescan.

Table 1
Results of fitting Eq. (3) to the Al- and Ga-signal of six EDX-linscans and there SNR.

Fitting results for the Al-K signal				
$d_{plateau}$ (nm)	$\Delta d_{edge,1}$ (nm)	$\Delta d_{edge,2}$ (nm)	R^2	SNR
157	51	39	0.96684	13.29
160	53	47	0.96827	13.29
159	44	47	0.94202	9.52
158	38	47	0.94842	10.41
153	30	25	0.91466	7.84
149	28	33	0.94432	9.88
Al-edge: average of six linescans				
156 ± 4	41 ± 10	40 ± 9		
Fitting results for the Ga-edge				
d_{EDX} (nm)	$\Delta d_{edge,1}$ (nm)	$\Delta d_{edge,2}$ (nm)	R^2	SNR
157	36	47	0.90242	7.09
159	45	42	0.87288	6.38
159	51	58	0.86316	6.05
153	33	41	0.82941	5.34
150	37	20	0.66844	3.44
155	33	50	0.82883	5.15
Ga-edge: average of six linescans				
156 ± 4	39 ± 7	43 ± 13		

For a more detailed investigation of the physical resolution limits using thin FIB-lamellas in EDX-analysis we performed Monte-Carlo simulations using a slightly modified version of the DTSA-II program written by Ritchie [10]. For all simulations we have assumed a Gaussian electron beam profile with a width of 1 nm and an acceleration voltage of 30 kV. Fig. 6 compares the spatial distribution of the generated characteristic X-rays at the Ga-K, the Al-K and the Au-L emission lines in a 100 nm thin GaAs, AlAs and Au lamellas respectively. It can be seen that only a cone shaped neck appears for the simulation of GaAs and AlAs, which causes a significant gain in resolution compared to classical bulk

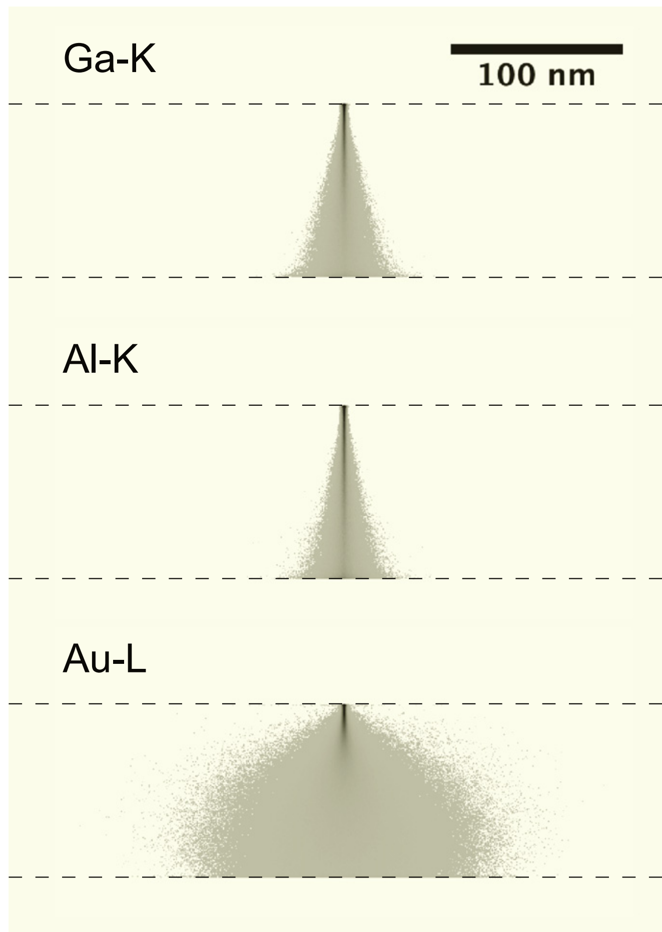

Fig. 6. Spatial distribution of the generated Ga-K, Al-K and Au-L X-ray emissions respectively in a GaAs, AlAs and a Au sample with 100 nm thickness calculated by Monte-Carlo simulations.

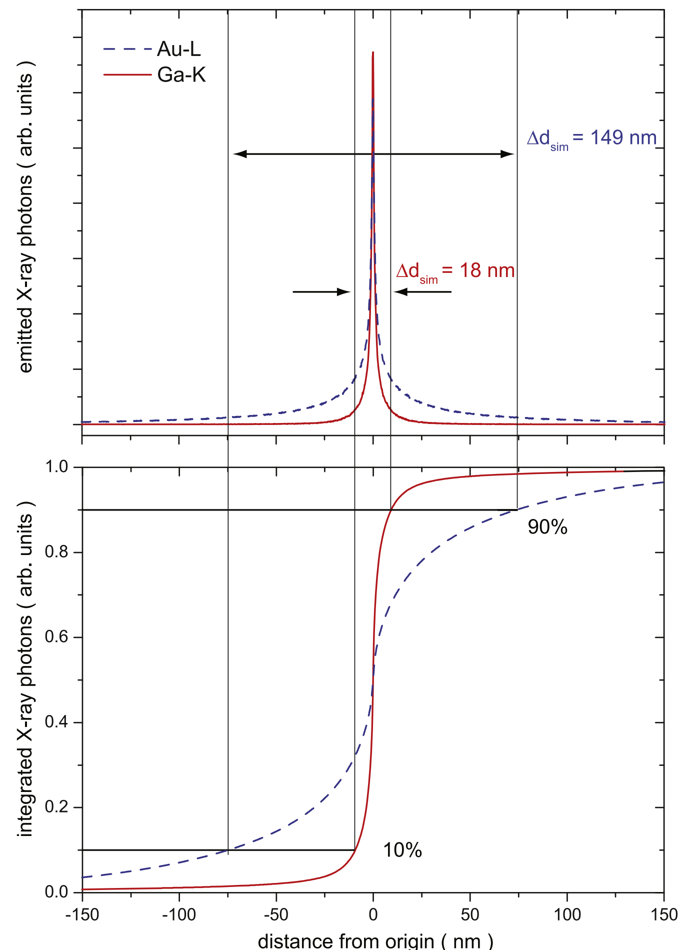

Fig. 7. Lateral X-ray distribution of the emitted Ga-K (solid red curve) and Au-L (dashed blue curve) intensities obtained from the Monte-Carlo simulations shown in Fig. 6. The Au signal is scaled by a factor of 2. The horizontal lines indicate the distance, where the signal increases from 10% to 90% of the step height. (For interpretation of the references to color in this figure caption, the reader is referred to the web version of this article.)

samples under identical conditions. For the Monte-Carlo simulation of Au the development of a tear-drop like excitation volume as expected for bulk samples becomes visible. To obtain a resolution from the Monte-Carlo simulations which is consistent with the experimental edge resolution described above, we extract the lateral X-ray emission profile and integrate it along the *x*-axis as shown in Fig. 7 (bottom), which is a good approximation of scanning across a sharp material interface. Again we define the edge resolution Δd_{sim} as the distance between the points where the EDX signal increases from 10% to 90% of the step height (indicated as horizontal lines in Fig. 7). With this definition we obtain an edge resolution of $\Delta d_{sim} = 19$ nm for the Ga-K and $\Delta d_{sim} = 149$ nm for the Au-L emission. The numerically determined edge resolution matches the experimental within a factor of 2 ($\Delta d_{sim} = 19$ nm and $\Delta d_{exp} \approx 40$ nm). The difference between the experimental and simulated edge resolution can be attributed either to the mean signal-to-noise ratio, an electron beam induced degeneration of the sample or to a residual image shift during the linescan. Linescans with an increased measurement time, and thus a better SNR lead to a deterioration of the resolution (not shown). A residual image shift along the scan direction does not significantly alter the determination of the plateau width but the edge resolution and is therefore consisted with the experimentally observed high resolution of $\Delta d_{plateau} \pm$ 4 nm for the Al-rich plateau width. For long measurement times we observe the growth of a carbon film on top of the FIB-lamella (see e.g. Fig. 1), which can in principal also alter the resolution. The carbon contamination should influence both the edge resolution and the measurement of the plateau width in the same way. The high resolution of $\Delta d_{plateau} \pm 4$ nm for the Al-rich plateau width indicates that the carbon layer has no significant influence for the short measurement times of the EDX-linescans. Therefore,

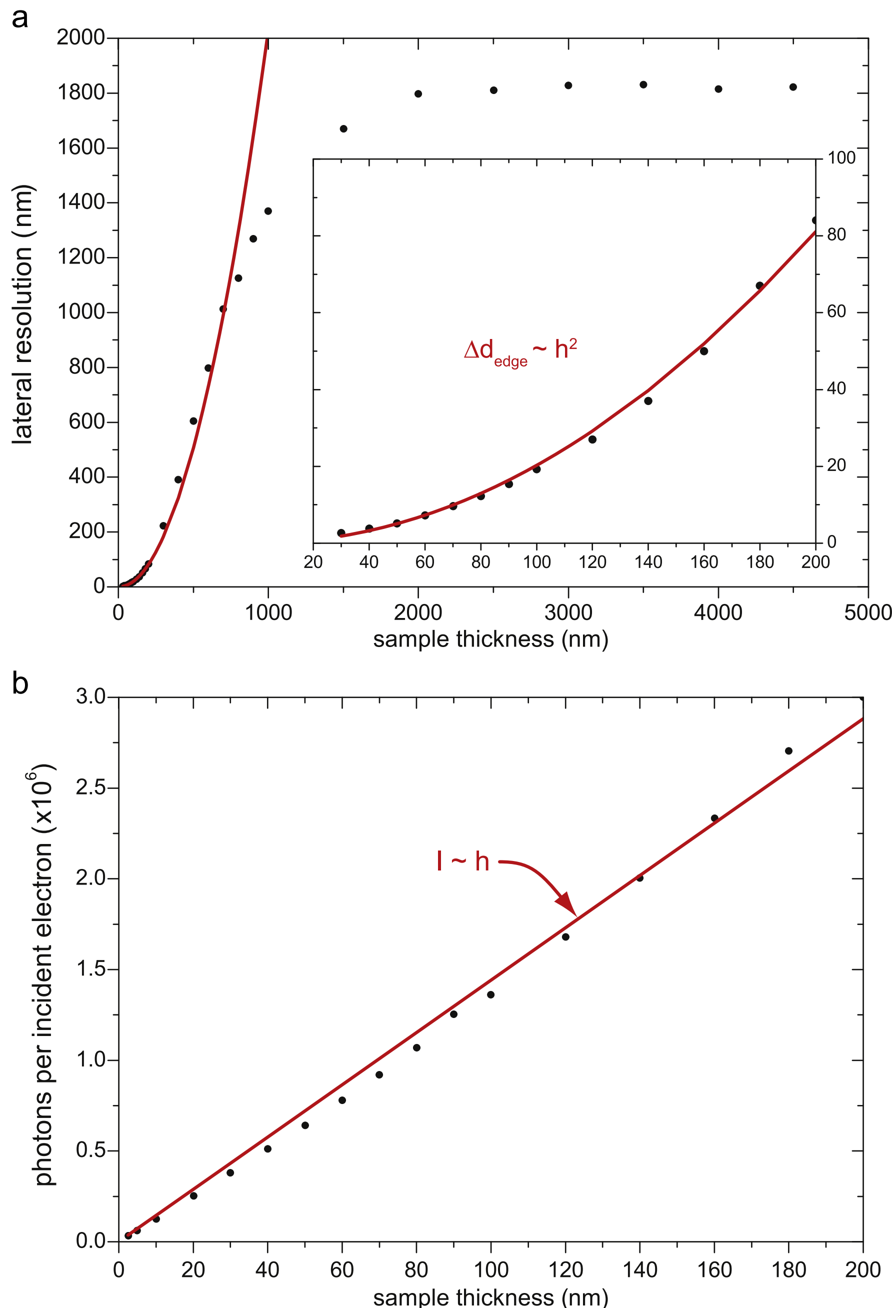

Fig. 8. Lateral resolution as a function of sample thickness (a) and the corresponding intensity of the emitted X-rays (b) obtained from Monte-Carlo simulations of a GaAs sample.

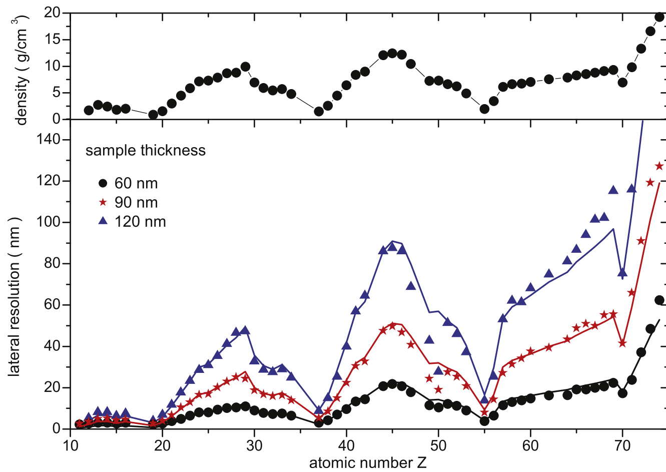

Fig. 9. Lateral resolution limit as a function of the atomic number Z (circles, stars and triangles) for different sample thicknesses (60 nm, 90 nm and 120 nm) (bottom) and the density of the elements as a function of Z (top). The lines represent the empirical formula (Eq. (4)) described in the text.

it is more likely that an uncompensated image drift (caused most probably by a small variation in the beam current, which cannot be compensated by the drift correction implemented in the EDX-software) degrades the edge resolution and is the limiting factor of the resolution rather than the signal-to-noise ratio or a degeneration (carbon contamination) of the sample.

Monte-Carlo simulations of a GaAs sample were performed for different sample thicknesses ranging from 10 nm to 4000 nm. Fig. 8 shows the resulting lateral resolution as a function of the lamella thickness. For thin lamellas (<200 nm) the Monte-Carlo simulation reveals a parabolic dependence (solid line), whereas at large sample thickness (>2000 nm) a saturation is observed. The drawback of thin lamellas is a reduction of the signal intensity with decreasing sample thickness. In contrast to the parabolic dependence of the lateral resolution limit, the signal intensity scales nearly linear at small sample thicknesses (see Fig. 8b). Therefore, it is essential to optimize sample thickness, measurement time and beam current very carefully to obtain the highest lateral resolution together with suitable counting statistics in the EDX-experiment.

Furthermore, we have investigated the influence of the material on the resolution limit, for pure elements from sodium to mercury ($Z=11-75$). The results of the Monte-Carlo simulations are shown in Fig. 9 for three different sample thicknesses (60 nm, 90 nm and 120 nm). We suggest the following relation for an analytical description of the resolution limit as a function of the material parameter, atomic number Z, atomic mass A and density ρ

$$\Delta d_{edge}\,(\text{nm}) = \alpha(h)\cdot(Z\cdot(Z+1))\cdot\frac{\rho}{A}, \tag{4}$$

where $\alpha(h)$ is an empirical function to take into account the sample thickness h. The term $Z\cdot(Z+1)$ represents both the elastic and inelastic scattering cross-sections of a pure element with the atomic number Z (see e.g. Refs. [12,13]) while the term ρ/A describes the number of atoms in a unit volume. With a Levenberg–Marquardt method adapted from "Numerical Recipes in C" [14] we are able to fit Eq. (4) with respect to $\alpha(h)$ for all materials at the same time and obtain a reasonable fit with $\alpha(h)=25\,223.8\times 10^9\ \text{m}^2/\text{kg h}^2$, displayed as solid lines in Fig. 9. All features in the Monte-Carlo simulation are reproduced with the suggested ansatz, only slight deviations are observed for the elements 44–47 and above $Z=55$ for the 90 nm thick lamella. The minima in the curve are due to density variations of the elements (see inset of Fig. 9). The underestimated resolution for the 90 nm and 120 nm thick lamella at high Z values by Eq. (4) can be explained by multiple scattering events which become more imported at high Z values and results in the development of the classical tear-drop like X-ray excitation volume in the bulk limit. For the elements 44–47 the same argument seems to be valid, except that the high density instead of the atomic number causes the increased multi-scattering probability. Previous works [3,11], investigating EDX resolution using TEM's, predict a $h^{3/2}$ dependence of the resolution on the sample thickness for thin lamellas. Our Monte-Carlo simulations do not confirm this $h^{3/2}$ dependence, while the data presented in Fig. 8 can be fitted with a $h^{3/2}$ dependence and it is not possible to obtain a reasonable fit for all materials (shown in Fig. 9) at the same time. The origin of the parabolic dependence on the sample thickness is not yet fully clear.

4. Conclusion

In conclusion we have demonstrated high spatial resolution EDX-measurements in a JSM-7500F SEM utilizing a thin FIB-lamella, where the plateau width of the Al-rich area is reproduced within ± 4 nm and the experimentally determined edge resolution ($\Delta d_{edge}=40\pm 10$ nm) is up to a factor of 2 close to the physical limit estimated with the Monte-Carlo simulations ($\Delta d_{sim}\sim 19$ nm). From Monte-Carlo simulations, we find a parabolic relationship between the sample thickness and the resolution (Δd_{edge}). Furthermore, the Monte-Carlo simulations of pure elements ranging from $Z=11$ to $Z=75$ can be very well described with Eq. (4), where only the broadening of the incident electron beam due to elastic and inelastic scattering events is taken into account. This allows us to approximate the resolution of EDX-measurements on thin samples with a very simple formula, like the Castainge's formula for bulk samples at University Duisburg-Essen.

Acknowledgments

We would like to thank Robert Young and Manus Hayne from the Lancaster University for the growth of the heterostructure. Also, we wish to acknowledge the support of Axel Lorke at University Duisburg-Essen.

References

[1] John J. Friel, Charles E. Lyman, Microscopy and Microanalysis 12 (2006).
[2] L.J. Allen, A.J. D'Alfonso, B. Freitag, D.O. Lenov, MRS Bulletin 37 (2012) 47.
[3] D.B. Williams, J.R. Michael, J.I. Goldstein, A.D. Roming Jr., Ultramicroscopy 47 (1992) 121.
[4] I. Barkshire, P. Karduck, W.P. Rehbach, Silvia Richter, Mikrochimica Acta 132 (2000) 113.
[5] R. Castaing, Advances in Electronics and Electron Physics 13 (1960) 317.
[6] T. Sakurada, S. Hashimoto, Y. Tsuchiya, S. Tachibana, M. Suzuki, K. Shimizu, Journal of Surface Analysis 12 (2005) 118.
[7] M. Halvarsson, T. Jonsson, S. Canovic, Journal of Physics: Conference Series 126 (2008) 012075.
[8] G. Cliff, G.W. Lorimer, Journal of Microscopy 103 (1975) 203.
[9] In principle any sufficiently smooth step-function can be used to fit the data to make the evaluation process more objective. We have chosen a Fermi-Dirac-function because one obtains easily the center position and width of the 10% to 90% signal increase in an analytic form.
[10] N. Ritchie, "DTSA-II", 〈http://www.cstl.nist.gov/div837/837.02/epq/index.html〉, 2010.
[11] E. Van Cappellen, Albrecht Schmitz, Ultramicroscopy 41 (1992) 193.
[12] L.A. Kulchitsky, G.D. Latyshev, Physical Review 61 (1942) 254.
[13] K. Murata, T. Matsukawa, R. Shimizu, Japanese Journal of Applied Physics 10 (1971) 678.
[14] W. Press, S. Teukolsky, W. Vetterling, B. Flannery, Numerical Recipes in C, 2nd ed., Cambridge University Press, Cambridge, UK, 1992.